Elements and Applications of Scale-Resolving Simulation Methods in Industrial CFD

F. Menter

1 Introduction

Historically, industrial CFD simulations have been based on the Reynolds Averaged Navier-Stokes Equations (RANS). For many decades, the only alternative to RANS was Large-Eddy Simulation (LES), which has however failed to provide solutions for most flows of engineering relevance due to excessive computing power requirements for the simulation of wall-bounded flows. On the other hand, RANS models have shown their strength essentially for wall-bounded flows, where the calibration according to the law-of-the-wall provides a sound foundation for further refinement. For free shear flows, the performance of RANS models is much less uniform. For this reason, hybrid models are gaining acceptance, where large eddies are only resolved away from walls and where the wall boundary layers are entirely covered by a RANS model e.g. Detached Eddy Simulation DES [1] or Scale-Adaptive Simulation SAS [2].

Such simulations are possible today for industrial-scale applications on medium sized computing systems (100–1,000 cores) and make their way into the industrial environment. These models are typically applied to flows with strong flow instabilities which cover a wide range of applications. Examples are the simulation of heat-transfer phenomena [3], acoustic stimulations [4] or gas turbine simulations [5]. The grids used in such simulations are typically in the range of 10^7–10^8 and therefore not drastically larger than high quality RANS meshes. The increase in computing costs results mainly from a need to integrate the equations in the time domain. This requires sufficiently long running times for establishing a proper flow-field and for allowing sufficient time for statistical averaging.

F. Menter (✉)
ANSYS Germany GmbH, Otterfing, Germany
e-mail: florian.menter@ansys.com

J. Fröhlich et al. (eds.), *Direct and Large-Eddy Simulation IX*,
ERCOFTAC Series 20, DOI 10.1007/978-3-319-14448-1_24

While these methods can lead to a significant increase in accuracy, their application is still not a routine procedure in most companies, partly due to the intricacies in mesh generation and simulation setup and partly because of the long turn-around-time. Nevertheless, such methods are well on their way of gaining acceptance into the industrial design cycle within the next few years.

A further step in hybrid modeling involves the resolution of parts of the turbulence inside of wall boundary layers. Due the well-known resolution demands of classical wall-resolved LES, industrial methods aim at the application of a RANS model in the innermost part of the wall boundary layer and then to switch to an LES model for the main part of the boundary layer [6]. Such models are termed Wall Modelled LES (WMLES). It can be shown that this approach avoids/reduces the unfavorable Reynolds number scaling of classical LES, which results from ever decreasing scales (with increasing Reynolds number) close to the viscous sublayer. While such models are available in advanced industrial CFD codes, their exploration as industrial CFD tools is just starting. There are several reasons for that. The first being that RANS models are fairly strong in predicting attached and mildly separated boundary layers. The second is that the CPU power required for WMLES is still too high for most applications to be practical for complete configurations. However, such methods can be used for studying reduced parts of the flow domain, either in separation or in the framework of an embedded or zonal LES method.

Another essential element of Scale-Resolving Simulations (SRS) are methods for generating resolved turbulence structures at inlets to the LES domain. This is most conveniently achieved by synthetic turbulence generated from the information from the upstream RANS model. One of the methods favored by the authors group is the Vortex Method [7], which offers a fair compromise between complexity and accuracy.

Finally, for large domains, it is frequently only necessary/possible to cover a small portion with Scale-Resolving Simulation (SRS) models, while the majority of the flow can be computed in RANS mode. In such situations, zonal or embedded LES methods are attractive e.g. [8, 9]. Such methods are typically not new models in the strict sense, but allow the combination of existing models/technologies in a flexible way in different zones of the simulation domain. Important elements of zonal models are interface conditions, which convert turbulence from RANS mode to resolved mode at pre-defined locations. In most cases, this is achieved by introducing synthetic turbulence based on the length and time scales from the RANS model, however with direct coupling with the upstream RANS model.

The challenge for the engineer is to select the most appropriate model for the intended application. Unfortunately, none of the available SRS models is able to efficiently cover all industrial flows. A compromise has to be made between generality and CPU requirements. The paper will discuss the main modeling approaches available in todays industrial CFD codes and provide some guidelines as to their optimal usage. Numerous examples of validation cases will be shown and the pros and cons of the different methods will be highlighted.

2 Elements of Hybrid RANS-LES Turbulence Models

In this chapter, different elements and aspects of modeling industrial flows with hybrid RANS-LES methods will be discussed, focusing on formulations favored by the authors group.

2.1 Global RANS-LES Hybrid Model Formulation

The authors group focuses on two types of global hybrid RANS-LES models, namely, Detached Eddy Simulation (DES) and Scale-Adaptive Simulation (SAS). The first is an explicit blend of RANS and LES based on the ratio of the turbulence length scale and the grid spacing. The second is a so-called second generation URANS model, which does not involve the grid spacing explicitly in the RANS formulation. Both formulations have their advantages and disadvantages.

The main potential problem with DES is that the RANS solution can be affected by the grid spacing. If that happens inside boundary layers, the result is often "Grid-Induced Separation (GIS)" [10]. In order to protect the boundary layer from this effect, the use of shielding functions has been proposed [10] and later adopted by [11]. The resulting model is termed Delayed Detached Eddy Simulation (DDES). It should be noted that shielding can only reduce the problem, but not eliminate it. This means that GIS can still happen in case of strong mesh refinement. Without shielding, the problem appears approximately if $\Delta_{\max} < \delta$ and with shielding if $\Delta_{\max} < 0.2\delta$ ($\Delta_{\max}$ being the max. edge length of a local cell and δ the local boundary layer thickness) [12]. In addition, DDES can show "grey zones", where the model does operate neither in RANS nor in LES mode. This can happen either, because the grid resolution is not sufficient for LES (but already affects the RANS model) or when there is insufficient instability in the flow to generate turbulence structures quickly enough in the zone of interest.

The main potential problem with SAS is that it can remain in (U)RANS mode, even though the user is interested in a scale-resolved simulation. This situation occurs in flows, which do not show a strong enough flow instability to push the model into the LES regime [13].

2.2 Models for Large Eddy Simulation (LES)

There is a variety of model formulations for LES implemented in the ANSYS CFD codes.

- Smagorinsky (standard and dynamic [14, 15])
- k-equation based model (dynamic [16])
- WALE model [17]
- Wall Modelled LES (WMLES, [18])

In industrial CFD (and not only there) the LES models of choice are eddy-viscosity formulations. Their main purpose is to provide proper dissipation at the small scales. This is in principle not a very demanding task and can be achieved by all models listed. LES model selection is therefore much less demanding on the user than RANS model selection. However, the standard Smagorinsky model has the disadvantage that it does not provide zero eddy-viscosity for simple shear flows (laminar flows, viscous sublayer). This problem is avoided by the dynamic and the WALE model. Due to some of the conceptual problems of the dynamic modeling approach (need for averaging, potentially negative eddy-viscosities, large variation of dynamic coefficient), the more optimal choice in this authors opinion is the WALE model.

Wall Modelled LES (WMLES) models are a fairly new member of industrial LES formulations. Their main goal is to allow integration to the wall, even at high Reynolds numbers, without the excessive grid resolution requirements of classical wall-resolved LES. WMLES is based on the concept of covering the inner portion of the boundary layer by a RANS and the outer portion by a LES formulation. This avoids the very high resolution requirements of LES in the inner wall layer. A very simple and promising approach to WMLES has been proposed by Shur et al. [18]. It is based on a reformulation of the length scale used in the LES zone and by blending it with the mixing length (RANS) model in the inner part of the boundary layer. The formulation of Shur et al. is given by:

$$\nu_t = \min\left\{(\kappa d_W)^2\,,\,(C_{SMAG}\Delta)^2\right\}\left\{1-\exp\left[-\left(y^+/25\right)^3\right]\right\}S \qquad (1)$$

where d_W is the wall distance, S is the shear strain rate and Δ a measure of the cell size. This model was originally calibrated for a 4th order central difference scheme (Shur et al. [18]), and needs to be lightly adjusted for lower order schemes.

2.3 Periodic Channel Flow

Simulations were carried out for periodic channel flows on grids with the characteristics given in Table 1. The domain size was $LX = 16h$, $LY = 2h$, $LZ = 3h$ (h being half the channel height—this corresponds approximately to the boundary layer thickness for wall boundary layers). The main characteristics of WMLES is clearly visible from Table 1: the non-dimensional values for $\Delta X+$ and $\Delta Z+$ are far beyond the limits of standard LES methods (which are $\Delta X+ = 40$, $\Delta Z+ = 20$). For WMLES, one only has to ensure a minimum number of cells per boundary layer volume $\delta \times \delta \times \delta$. In the current formulation the minimum resolution per boundary layer volume is of the order of $10 \times 40 \times 20$ cells (streamwise, normal and spanwise).

Figure 1 shows the velocity profiles in logarithmic scale for these simulations using ANSYS-Fluent. It is well known that the use of hybrid models like DES can result in a strong log-layer mismatch and a corresponding error in the wall shear stress when applied as a WMLES model. Figure 1 shows that the log-layer miss-match

Table 1 Grids for periodic channel flow at different Reynolds number using WMLES

Re_τ	Cells	Nodes	$\Delta X+$	$\Delta Y+$	$\Delta Z+$
395	384,000	81 × 81 × 61	040.0	0.2 ÷ 30	20.0
395	1,764,000	141 × 141 × 91	026.6	0.2 ÷ 20	13.3
760	480,000	81 × 101 × 61	76.9	0.2 ÷ 30	38.5
1,100	480,000	81 × 101 × 61	111.4	0.2 ÷ 30	55.7
2,400	528,000	81 × 111 × 61	243.0	0.2 ÷ 30	121.5
18,000	6,240,000	81 × 131 × 61	1822.7	0.2 ÷ 30	911.4

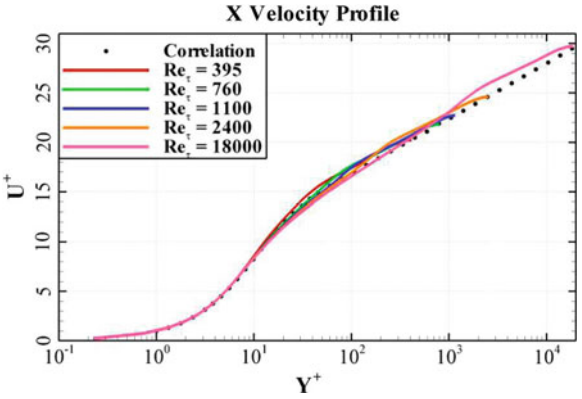

Fig. 1 Velocity profiles in logarithmic scale for periodic channel flow using WMLES for various Reynolds numbers

can be reduced to a relatively small shift at the RANS-LES interface, resulting in a high quality solution even at very high Re numbers for the above formulation (see also [18]).

2.4 Flat Plate Boundary Layer

A more challenging test case is the flow over a flat plate boundary layer, where the boundary layer grows and where synthetic turbulence needs to be provided at the inlet. The grid for the boundary layer test case has the parameters given in Table 2.

Table 2 Grids for boundary layer flow at different Reynolds number using WMLES

Re_Θ	Cells	Nodes
1,000/10,000	1,050,000	251 × 71 × 62

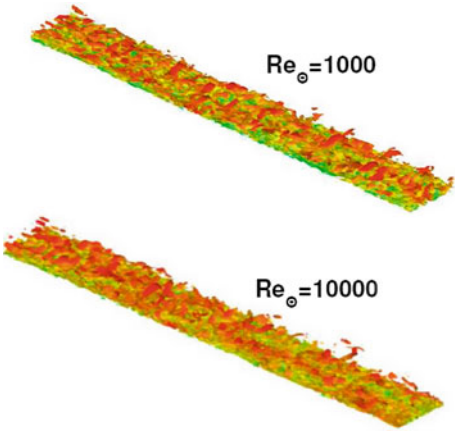

Fig. 2 Turbulence structures for wall boundary layer flow. *Top* $Re_\Theta = 1{,}000$, *Bottom* $Re_\Theta = 10{,}000$

Figure 2 shows the turbulent structures for a wall boundary layer flow using the WMLES option. Again the outer part is covered by LES and the near wall part by RANS. The flow was computed with ANSYS-Fluent and the turbulence at the inlet was generated by the Vortex Method (e.g. [19]). The turbulence was well maintained as can be seen from Fig. 2. In Fig. 3 the wall shear stress is displayed. The WMLES recovers quickly from the synthetic turbulence and maintains a proper wall shear stress downstream.

Figure 4 shows the velocity profile of a simulation for the boundary layer at $Re_\Theta = 10{,}000$. Such a Re number is typically out of reach for wall-resolved LES due to the large grid resolution required. In the present study a grid with only $\approx 1.3 \times 10^6$ cells was used ($\Delta x+ \approx 700$, $\Delta z+ \approx 350$). Synthetic inlet turbulence was generated using the Vortex Method. The logarithmic layer is captured very well as seen in Fig. 4.

It should be noted that WMLES is still substantially more computationally expensive than RANS. However, it avoids the excessive Re number scaling of classical wall-resolved LES and allows the simulation of limited parts of technical devices at high Reynolds numbers for which RANS model simulations are not of sufficient accuracy.

2.5 Zonal RANS-LES Models

As pointed out in the previous sections, hybrid models like DES and SAS rely on flow instabilities to generate turbulent structures in large separated regions without the explicit introduction of unsteadiness through the boundary conditions. However, there are situations, where such instabilities are not present or are not reliable to serve this purpose. In such cases, it is desirable to apply RANS and the LES models in predefined zones and provide clearly defined interfaces between them. At these interfaces, the modeled turbulent kinetic energy from the upstream RANS model is

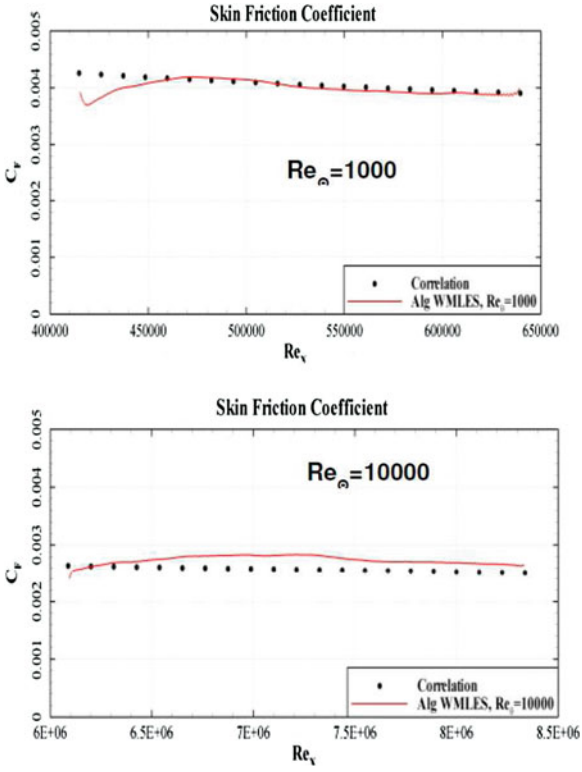

Fig. 3 Wall shear stress coefficient for wall boundary layer flow. *Top* $Re_\Theta = 1{,}000$, *Bottom* $Re_\Theta = 10{,}000$

converted explicitly to resolved scales at an internal boundary to the LES zone. The LES zone can then be limited to the region of interest where unsteady results are required. There are numerous zonal RANS-LES concepts, and it is not possible to cover all of them. The following results are therefore limited to the Embedded LES (ELES) method implemented in ANSYS-Fluent [8].

This approach has been selected as it is attractive from an industrial CFD perspective. It allows the user to pre-specify RANS and LES zones in a single CFD simulation. At the RANS-LES interface, the modeled turbulence from the RANS model is converted into resolved turbulence using the methods previously available for this purpose at inlets. ELES allows the selection of virtually all RANS models in the RANS domain and all algebraic LES models in the LES region. Figure 5 shows the application of ELES to a channel flow. The front portion of the channel is covered by the SST RANS model [20]. The RANS-LES interface uses the Vortex Method to convert modeled turbulence to resolved synthetic turbulence and the WALE LES [17] model to provide an LES eddy-viscosity. Downstream, the method switches back to RANS. The numerical method allows switching from Second Order Upwind to Central Difference between the RANS and the LES region.

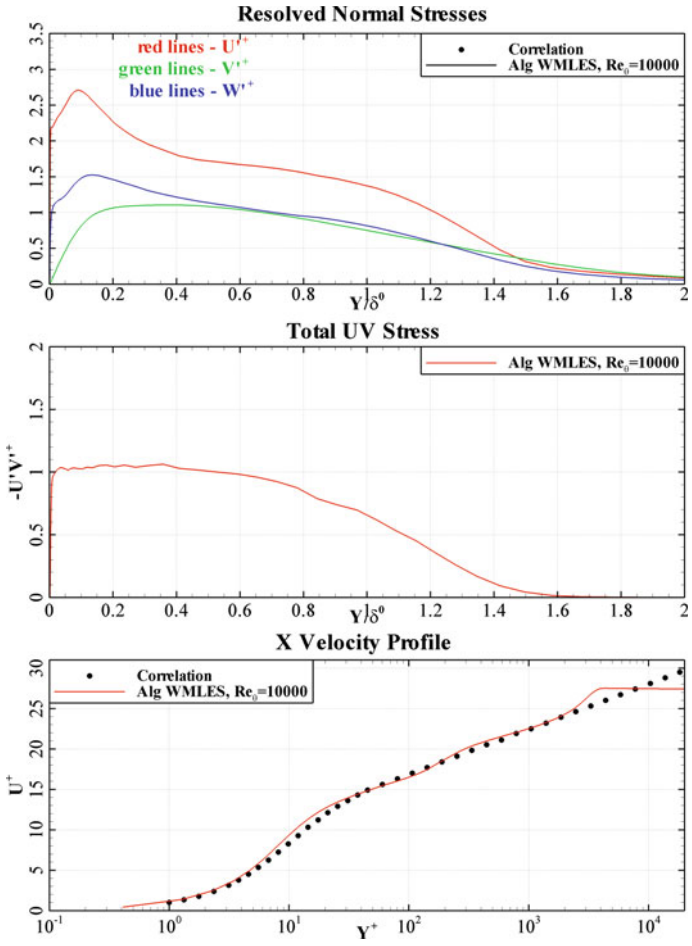

Fig. 4 Profile information for the flat plate boundary layer simulations. $Re_{\Theta} = 10{,}000$

Figure 6 shows a comparison of the LES results inside the embedded region with DNS data, both for the mean flow profile and the turbulence RMS values. The agreement is quite close, considering the limited length of the LES zone.

3 Application Examples

Numerous application examples will be shown. They typically originate from industry-specific validation projects/workshops in which the authors group has participated. Such test cases are characterized by reduced geometric complexity, but provide experimental data, typically not available for industrial applications.

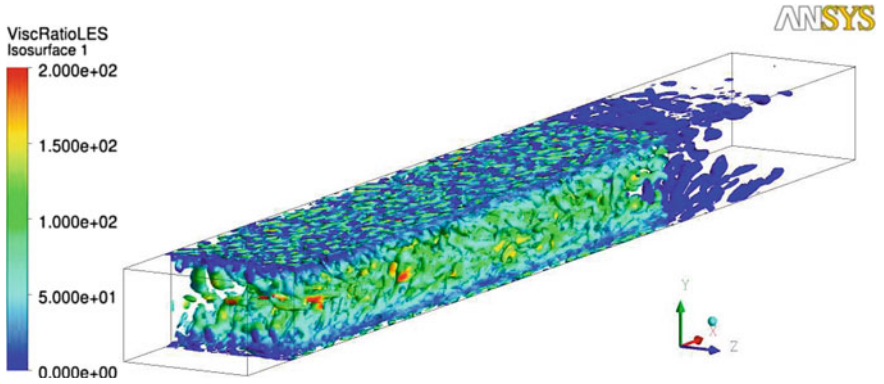

Fig. 5 Channel flow. Viscosity ratio on iso-surfaces of Q-criterion (−500)

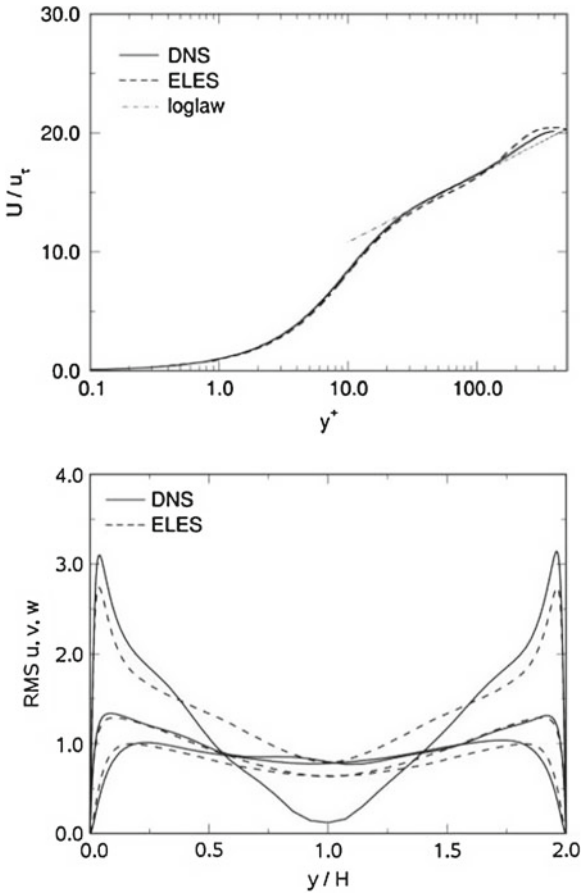

Fig. 6 Fully developed channel flow. Mean velocity values inside LES zone (*top*), rms values inside LES zone at $x = 1.5 + 1.5\pi$ (*bottom*)

3.1 Acoustic Cavity

Air flow past a 3-D rectangular shallow cavity was calculated in order to test the SAS models ability to predict correct spectral information for acoustics applications. The cavity geometry and flow conditions corresponding to the M219 experimental test case of Henshaw [21]. The experiment investigates the noise generation due to turbulent structures forming from the front lip of the cavity and interacting with the cavity walls.

Figure 7 shows the turbulent structures, produced by the SST-SAS model (iso-surface Q-criterion). The power spectral density (PSD) of the transient pressure signals calculated and measured by sensors on the cavity bottom near the leading and the downstream wall respectively is plotted in Fig. 8. These plots show that the PSD levels are captured in good agreement with the data. Similar agreement was achieved for the other experimental locations (not shown here) Kurbatskii et al. [22].

3.2 NACA 0021 Airfoil Beyond Stall

This low Mach number flow around a symmetric NACA 0021 airfoil was experimentally investigated by Swalwell et al. [23]. The flow is characterized by a massive separation zone behind the airfoil. The experiment was carried out at a high angle of attack of $\alpha = 60°$ and at a chord-based Reynolds number of $Re = 2.7 \times 10^5$.

The spanwise extension of the computational domain was selected to be four chord-lengths for this calculation, and an O-type hexahedral grid with $140 \times 101 \times 134$ nodes, provided for the DESider consortium, was used for the SST-SAS simulation with the ANSYS-CFX solver. A timestep equal to 3 % of the convective timescale (chord length over the inlet velocity magnitude) was used. This corresponds to a Courant number of about unity in the separated zone just downstream of the airfoil.

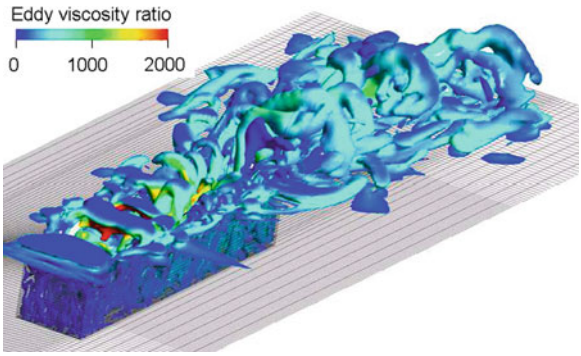

Fig. 7 Resolved turbulent structures for cavity flow: iso-surface $\Omega 2 - S2 = 5 \times 105\ s - 2$

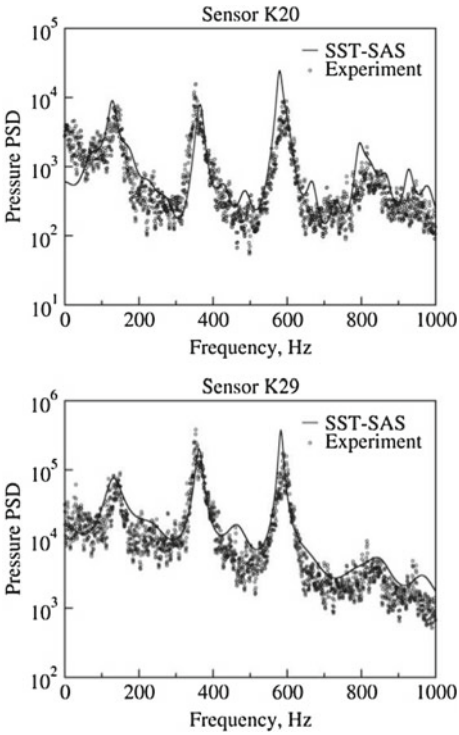

Fig. 8 Power spectral density of the transient wall pressure signals on the cavity *bottom left* sensor K20 located close the front wall, *right* sensor K29 located close to the rear wall

Figure 9 shows a comparison of the computed and the experimental pressure distributions. The agreement is good and within the range of other simulations in the DESider project. Figure 10 shows the turbulent structures (iso-surface Q-criterion) computed by the SST-SAS model behind the airfoil. The structures are essentially resolved down to the grid limit with the larger structures indicating the grid coarsening away from the airfoil. Unsteady SST simulations show the typical single-mode vortex separation expected from classical URANS models.

The experience gained during the simulation of this flow showed the importance of sufficiently long physical time integration for the correct prediction of the average surface pressure and for the low-frequency part of the spectra of forces. During the reported simulation, about 400 convective units based on chord length have been run for the transient statistics after first establishing the solution. In order to achieve better averaging, the spectra of forces have been calculated for each grid section separately and then averaged across the spanwise direction. Figure 11 shows the power spectral densities of the lift and drag coefficients, which are in good agreement with the data, demonstrating the correct temporal response of the model.

The integral lift and drag coefficients, presented in Table 3, are predicted with 2 % accuracy compared to the measurements. It should be noted that a slight dependency of these values on the spanwise size of the domain was observed by some partners in the DESIDER project. This ratio was not varied in the current simulations.

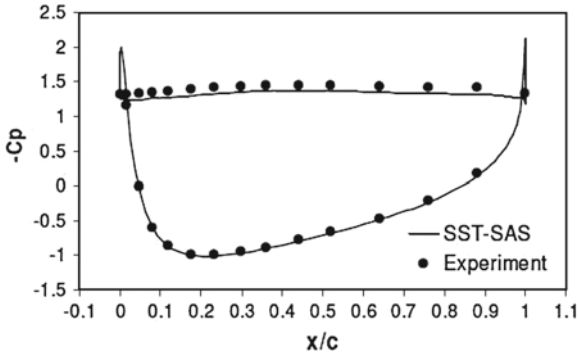

Fig. 9 Comparison of experimental and numerical wall pressure distribution

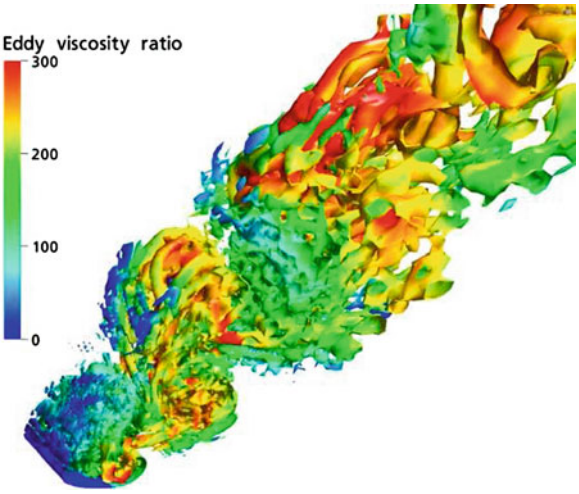

Fig. 10 SAS-resolved turbulent structures behind the airfoil

The good prediction of the power spectral densities for this test case using the SST-SAS model demonstrates the accuracy of the model in the time/frequency domain. In Refs. [2, 24] the SAS model is described in detail and is applied to a wide variety of generic and industrial-like flows.

3.3 Generic Fighter Aircraft

Figure 12 shows SAS simulations over a generic airplane geometry. The simulation ($Re = 2.8 \times 10^6$, $\alpha = 15°$) has been carried out on an unstructured mesh with 11×106 control volumes. The upper part shows the geometry and the turbulent structures produced by the simulation. The lower part shows a comparison between the experimental data and the time averaged simulation. The simulation is in good agreement with the exp. data [25].

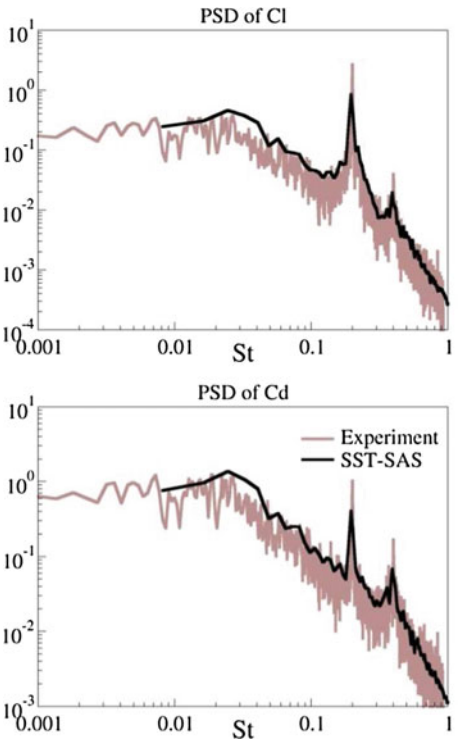

Fig. 11 Turbulent spectra of forces for NACA0021 airfoil: *top* power spectral density of the lift coefficient, *bottom* power spectral density of the drag coefficient

Table 3 Lift and drag coefficients for the NACA 0021 at 60° angle of attack

	Lift coefficient, CL	Drag coefficient, CD
SST-SAS	0.915	1.484
Experiment	0.931	1.517

3.4 Heat Transfer in T-Junction

The following example is a flow through a pipe T-junction with two streams at different temperatures. This testcase was a used as a benchmark of the OECD to evaluate CFD capabilities for reactor safety applications [26]. The geometry and grid are shown in Fig. 13a, b. The grid consists of ≈5 million hexahedral cells. This flow is not easily categorized. In principle it can be computed with SAS and DDES models in SRS mode (not shown). This means that the instability in the interaction zone between the two streams is sufficiently strong to generate unsteady resolved turbulence. However, it was also observed, that these simulations are extremely sensitive to the details of the numerical method employed or the shielding function used. The SAS model provided "proper" solutions only when a pure Central Difference scheme was selected, but remained in URANS mode in case of the Bounded Central Difference scheme. The DDES model provided correct solutions, when a non-conservative

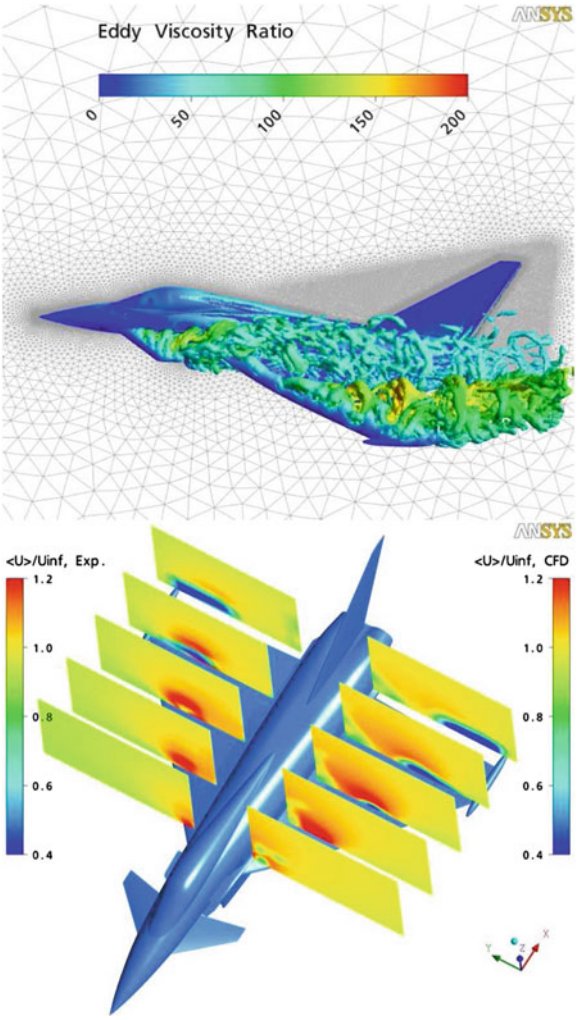

Fig. 12 Flow over generic airplane configuration FA-5. *Top* flow structures. *Bottom* comparison of exp. and SAS axial flow component (Geometry and data are Courtesy of EADS Deutschland)

shielding function was used but produced only weak unsteadiness in case of a conservative shielding function. It is therefore better to apply the ELES model, where modeled turbulence is converted into synthetic resolved turbulence in both pipes upstream of the interaction zone at pre-defined RANS-LES interfaces. In addition, the turbulence model was switched from SST to WMLES at these interfaces. This approach then avoids the need for the flow instability of the interacting streams to generate resolved scales.

Figure 13c shows that the resolved turbulence starts already upstream of the interaction zone due to the introduction of synthetic turbulence. Figure 13d shows a comparison of computed and experimental axial velocity profiles in the main pipe at

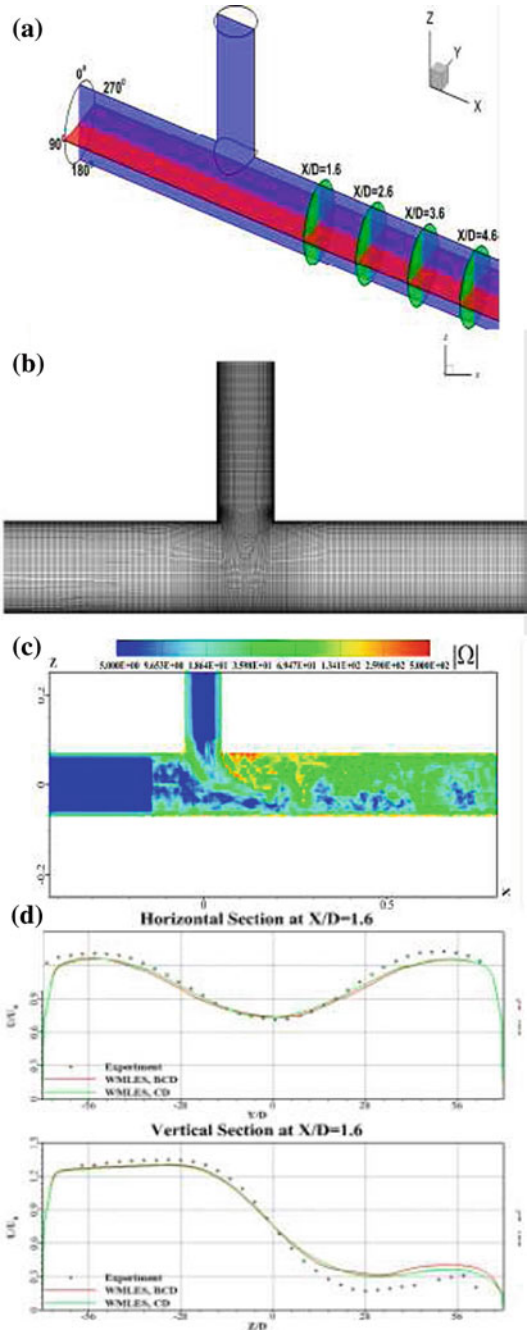

Fig. 13 T-Junction simulation. **a** Geometry. **b** Grid. **c** turbulence structures. **d** Axial velocity at station $X/D = 1.6$ for *horizontal* and *vertical lines*

$X/D = 1.6$. The method provides a good agreement between the simulations and the experimental data. It can also be seen that the switch from CD to BCD does not affect the solutions. This is different from the observation with the SAS model, which reacts sensitive to such changes in the current testcase.

4 Summary

An overview of Scale-Resolving Simulation (SRS) technologies developed for the ANSYS CFD codes was presented. The underlying principles, as well as some of the pros and cons of different modeling approaches haven been discussed. Numerous genetic and application-oriented examples have been shown.

References

1. Spalart, P.R.: Strategies for turbulence modelling and simulations. Int. J. Heat Fluid Flow **21**, 252 (2000)
2. Menter, F.R., Egorov, Y.: Scale-adaptive simulation method for unsteady flow predictions. Part 1: theory and model description. J. Flow Turbul. Combust. **85**(1), 113–138 (2010)
3. Duda, B.M., Menter, F.R., Deck, S., Bezard, H., Hansen, T., Esteve, M.-J.: Application of the scale-adaptive simulation to a hot jet in cross flow. AIAA. J. **51**(3), 674–685 (2013)
4. Langtry, R.B., Spalart, P.R.: Detached eddy simulation of a nose landing-gear cavity. In: IUTAM Bookseries, vol. 14 (2009)
5. Widenhorn, A., Noll, B., Aigner, M.: Numerical characterization of a gas turbine model combustor applying scale-adaptive simulation, GT2009-59038. In: Proceedings of ASME TURBO EXPO 2009
6. Shur, M.L., Spalart, P.R., Strelets, M.K., Travin, A.K.: A hybrid RANS-LES approach with delayed-DES and wall-modeled LES capabilities. Int. J. Heat Fluid Flow **29**, 1638–1649 (2008)
7. Mathey, F., Cokljat, D., Bertoglio, J.P., Sergent, E.: Specification of LES inlet boundary condition using vortex method. In: 94th International Symposium on Turbulence, Heat and Mass Transfer, Antalya (2003)
8. Cokljat D., Caradi, D., Link, G., Lechner, R., Menter, F.R.: Embedded LES methodology for general-purpose CFD solvers. In: Proceedings of Turbulent Shear Flow Phenomena, Proceedings of 6th International Symposium on Turbulence and Shear Flow Phenomena, Seoul, Korea, 22–24 June 2009, pp. 1191–1196 (2009)
9. Menter F.R., Garbaruk, A., Smirnov, P.: Scale adaptive simulation with artificial forcing. In: Proceedings of 3rd Symposium on Hybrid RANS-LES Methods (2009)
10. Menter, F.R., Kuntz, M.: Adaptation of eddy-viscosity turbulence models to unsteady separated flow behind vehicles. In: Proceedings of Conference the Aerodynamics of Heavy Vehicles, Trucks, Busses and Trains, Asilomar, CA, Springer (2003)
11. Spalart, P., Deck, S., Shur, M., Squires, K., Strelets, M., Travin, A.: A new version of detached eddy simulation. Resistant to ambiguous grid densities. J. Theor. Comput. Fluid Dyn. **20**, 181–195 (2006)
12. Gritskevich, M.S., Garbaruk, A.V., Schtze, J., Menter, F.R.: Development of DDES and IDDES formulations for the k-shear stress transport model. J. Flow Turbul. Combust. **88**(3), 431–449 (2012)

13. Menter, F.R., Gritskevich, M.S., Schtze, J.: Global vs. zonal approaches in hybrid RANS-LES turbulence modelling progress in hybrid RANS-LES modelling. Notes Numer. Fluid Mech. Multidiscip. Des. **117**(2012), 15–28 (2012)
14. Smagorinsky, J.: General circulation experiments with the primitive equations. Mont. Weather Rev. **91**, 99–165 (1963)
15. Lilly, D.K.: A proposed modification of the Germano subgrid-scale closure model. Phys. Fluids **4**, 633–635 (1992)
16. Schumann, U.: Subgrid scale model for finite-difference simulations of turbulent flows in plane channels and annuli. J. Comp. Phys. **18**, 376 (1975)
17. Nicoud, F., Ducros, F.: Subgrid-scale stress modelling based on the square of the velocity gradient tensor. Flow Turbul. Combust. **62**(3), 183–200 (1999)
18. Shur, M.L., Spalart, P.R., Strelets, M.K., Travin, A.K.: A hybrid RANS-LES approach with delayed-DES and wall-modeled LES capabilities. Int. J. Heat Fluid Flow **29**, 1638–1649 (2008)
19. Mathey, F., Cokljat, D., Bertoglio, J.P., Sergent, E.: Specification of LES inlet boundary condition using vortex method. In: 4th International Symposium on Turbulence, Heat and Mass Transfer, Antalya (2003)
20. Menter, F.R.: Two-equation eddy-viscosity turbulence models for engineering applications. AIAA J. **32**(8), 1598–1605 (1994)
21. Henshaw, M.J.: M219 cavity case, verification and validation data for computational unsteady aerodynamics. Technical report RTO-TR-26, AC/323(AVT)TP/19 (2000)
22. Kurbatskii, K.A., Menter, F., Schuetze, J., Fujii, A.: Numerical simulation of transonic cavity noise using scale-adaptive simulation (SAS) turbulence model. In: Inter-Noise 2011, September 2011
23. Swalwell, K.E., Sheridan, J., Melbourne, W.H.: Frequency analysis of surface pressures on an airfoil after stall. AIAA Paper 2003–3416 (2003)
24. Egorov Y., Menter F.R., Cokljat, D.: Scale-adaptive simulation method for unsteady flow predictions. Part 2: application to aerodynamic flows. J. Flow Turbul. Combus. **85**(1), 139–165 (2010)
25. Laschka, B., Ranke, H., Breitsamter, C.: Application of unsteady measurement techniques to vortical and separated flows. Z. Flugwiss. Weltraumforsch. **19**, 90–108 (1995)
26. Westin, J., Alavyoon F., Andersson, L., Veber, P., Henriksson, M., Andersson, C.: Experiments and unsteady CFD-calculations of thermal mixing in a T-junction. OECD/NEA/IAEA Workshop on the Benchmarking of CFD Codes for Application to Nuclear Reactor Safety (CFD4NRS), Munich Germany, pp. 1–15 (2006)